Journal of Alloys and Compounds 779 (2019) 900–907

Contents lists available at ScienceDirect

Journal of Alloys and Compounds

journal homepage: http://www.elsevier.com/locate/jalcom

3D printing of NdFeB bonded magnets with $SrFe_{12}O_{19}$ addition

Fang Yang [a, *], Xinyue Zhang [a], Zhimeng Guo [a], Siyang Ye [b], Yanli Sui [b], Alex A. Volinsky [c]

[a] Institute for Advanced Materials and Technology, University of Science and Technology Beijing, Beijing, 100083, China
[b] State Key Laboratory for Advanced Metals and Materials, University of Science and Technology Beijing, Beijing, 100083, China
[c] Department of Mechanical Engineering, University of South Florida, Tampa, FL 33620, USA

ARTICLE INFO

Article history:
Received 22 June 2018
Received in revised form
21 November 2018
Accepted 25 November 2018
Available online 27 November 2018

Keywords:
3D printing
NdFeB
Bonded magnets
$SrFe_{12}O_{19}$
Thermal ability

ABSTRACT

Rectangular, square, ring and horseshoe-shaped NdFeB bonded magnets with $SrFe_{12}O_{19}$ addition have been prepared by additive manufacturing, also known as 3D printing. The prepared NdFeB slurries with ferrite addition were deposited to form shaped parts using a 3D printer. Highly loaded pseudo-plastic printing slurries were employed to print bonded magnets with 98% of theoretical density. In the printed magnets with 20 wt.% strontium ferrite ($SrFe_{12}O_{19}$), good dimensional accuracy and surface quality were obtained with a relatively low surface roughness of ~6 μm. In addition, good coalescence without obvious defects or pores was observed, and the ultimate tensile strength was 12 MPa. The magnetic properties of the hybrid magnets decreased with the increase of $SrFe_{12}O_{19}$ content due to a lower volume fraction of the NdFeB powder and lower magnetic performance of the $SrFe_{12}O_{19}$ powder. Nevertheless, the coercivity temperature coefficient β increased from −0.4%/°C to −0.2%/°C with the $SrFe_{12}O_{19}$ content increase to 20 wt.%, indicating better thermal stability of hybrid magnets. The proposed method of fabricating NdFeB bonded magnets significantly reduces the manufacturing cost of complex-shaped magnets, enables efficient utilization of rear earth elements and broadens elevated operating temperature applications.

1. Introduction

Due to high energy density, NdFeB permanent magnets have a variety of clean energy applications, including wind turbines, hybrid and electric vehicles [1]. NdFeB magnets have been classified into sintered and bonded magnets. While sintered magnets retain full density and offer high energy product, bonded magnets exhibit the net-shape formability and intermediate energy product [2]. One fact about NdFeB magnets is their dependency on rare-earth (RE) elements, such as Nd, Dy and Tb [3,4]. Machining of NdFeB sintered magnets gives rise to manufacturing costs and RE resources waste [5]. For applications where the obtained magnetic properties are sufficient, NdFeB bonded magnets can help address these issues by minimizing post-manufacturing processing wastes while using smaller quantities of the RE materials [6,7]. NdFeB bonded magnets are typically obtained by blending magnetic powders with a polymer as a binder, and then molded into desired shapes by compression, extrusion, injection and calendaring with minimal or no post manufacturing machining [8–10].

Demands for NdFeB bonded magnets are expected to substantially increase in the clean energy industry. Nevertheless, there are still some drawbacks of the conventional fabrication techniques used for bonded magnets, such as specific tooling requirements for each design and limitations in shape flexibility and complexity [2,11]. Additive manufacturing (AM), also known as 3D printing, has received much attention because of the flexible manufacturing ability to translate complex-shaped geometries into 3D objects directly [12,13]. Its' main benefits involve freedom of design, mass customization, waste minimization and the ability to manufacture complex structures as well as single-unit production [14,15]. Owing to this unique fabrication method, AM is well-suited to fabricate NdFeB bonded magnets, which frequently require expensive and critical RE elements [16].

To date, the majority of the additive efforts have been carried out to print fiber-reinforced composites [17], rechargeable microbatteries [18], structural metals [19], and high-temperature ceramics [20]. Nevertheless, AM printing of magnets is still in its infancy. Very recently, extrusion printing of NdFeB bonded magnets has been explored [21–24]. Nylon bonded NdFeB magnets have been printed with a density of 3.57 g/cm^3, which is lower than the injection molded magnets (4.35 g/cm^3) [21]. Based on the fused

* Corresponding author.
E-mail address: yangfang@ustb.edu.cn (F. Yang).

https://doi.org/10.1016/j.jallcom.2018.11.335
0925-8388/

deposition modeling, polycaprolactone (PCL) bonded NdFeB magnets have been prepared by anti-gravitational 3D printing [22]. Direct-write 3D printing of epoxy-based NdFeB bonded magnets has been investigated. The density of the printed parts is 3.53 g/cm^3 [23]. Although AM printed NdFeB bonded magnets have been successfully fabricated, the as-printed magnets are porous and exhibit relatively low density. In addition, poor thermal stability is still one obstacle that limits their further applications at elevated temperatures.

Therefore, it is of interest to 3D print hybrid bonded magnets with a mixture of NdFeB and strontium ferrite. Due to the positive coercivity temperature coefficient β of pure strontium ferrite magnets, the hybrid magnets exhibit considerably lower β compared with pure NdFeB magnets [25]. As reported in the literature [26], hybrid NdFeB–SmFeN nylon composite bonded magnets have been printed by a large area AM system. However, to date, no related reports describe AM printing of hybrid NdFeB/$SrFe_{12}O_{19}$ bonded magnets. In this paper, highly loaded pseudo-plastic printing slurry was prepared to 3D print bonded magnets made from NdFeB base and strontium ferrite powder. The printing appearance, microstructure, and magnetic properties of printed NdFeB bonded magnets with strontium ferrite were also investigated.

2. Experimental procedure

2.1. Slurry preparation

The printing slurry in this study was comprised of the thermosetting epoxy resin (used as a binder, Kunshan Green Shield Chemical Company, Jiangsu, China), polyetheramine (acted as a latent curing agent, Kunshan Green Shield Chemical Company, Jiangsu, China), acetone (AR, Sinopharm Chemical Reagent Co., Ltd), and hybrid magnetic powder. Weight percentages of each constituent in the respective mixtures are shown in Table 1. The hybrid magnetic powder used for printing consisted of a mixture of melt-quenched MQP-15-9HD NdFeB powder (about 75 μm, Magnequench Co., Ltd, Tianjin) and strontium ferrite powder ($SrFe_{12}O_{19}$, about 1 μm, China Grirem Advanced Materials Co., Ltd). The fractions of NdFeB and $SrFe_{12}O_{19}$ powder in a mixture were as follows: 100/0 wt.%, 92/8 wt.%, 85/15 wt.%, 80/20 wt.%, 75/25 wt.%. Fig. 1 shows the appearance and the particle size distribution of the raw powders. To prepare the slurry, polyetheramine and acetone were first added into epoxy resin to produce a premixed solution. Then, the hybrid magnetic powder was added into the above-premixed solution and mixed in a planetary centrifugal mixer at atmospheric pressure for 60 s.

Table 1
Composition of the raw materials[a].

Raw materials	Content (wt.%)
Thermosetting epoxy resin	13.0
Polyetheramine	3.90
Acetone	–
Magnetic powder	83.1

[a] Of every 100 g slurry, 1 g of acetone was also added to aid in mixing and deposition which was not included in the weight fraction calculations.

2.2. 3D printing

A material jetting additive manufacturing process was employed to 3D print the bonded magnets using a printer, as shown in Fig. 2(a). At the start of printing, 3D models were designed and sliced into the printing code using the Slic3r tool path generation software. Second, the printing slurry was loaded into a plastic syringe barrel with a nozzle. The deposition was achieved through the application of air pressure, and the stage motion and pressure modulation were controlled by a computer system. Then, the nozzle continuously printed bonded magnets at a speed of 30 mm/s. Finally, after printing onto substrates, the printed parts were cured at ambient temperature for 24 h. Fig. 2(b) lists a schematic diagram for printing NdFeB-based bonded magnets.

2.3. Testing and characterization

The density of the printed magnets was determined by the Archimedes' type measurements. The tensile testing of the dog-bone shaped specimens was carried out according to the ASTM D638 standard. Five samples for each processing condition were tested to confirm reproducibility. The room temperature magnetic properties were measured by a magnetic measurement device (NIM-200C). The powder particle size was measured by a laser particle analyzer (BT-9300S, Dandong Better Co. Ltd., China). The surface roughness and morphology of the printed magnets were measured by a confocal laser scanning microscope (CLSM, OLYMPUS LEXT OLS4100). The space between the printed lines was calculated by contrasting the scale bar and further verified according to the CLSM images analysis by an image analyzer (Nano Measurer Tool). Microstructure and fracture were characterized by backscattered electron scanning microscopy (FESEM, Supra55), combined with energy dispersive spectroscopy detector (EDS).

3. Results and discussion

3.1. 3D printing appearance

To investigate the $SrFe_{12}O_{19}$ effects on the printing appearance of 3D printed magnets, simple rectangular blocks were printed, as shown in Fig. 3. Due to the high density (about 7.6 g/cm^3) and

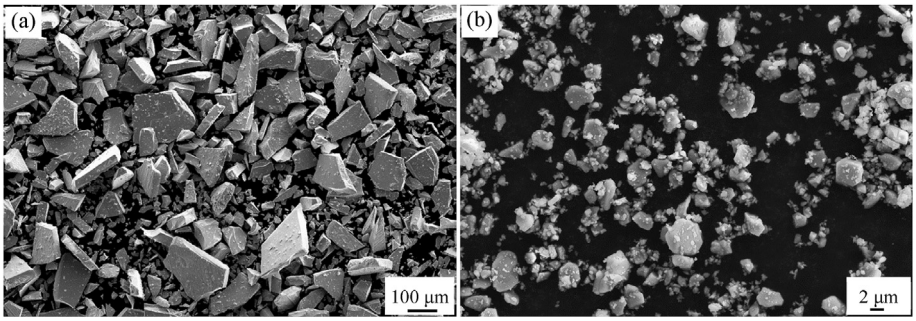

Fig. 1. SEM images of raw material powders: (a) NdFeB, (b) $SrFe_{12}O_{19}$.

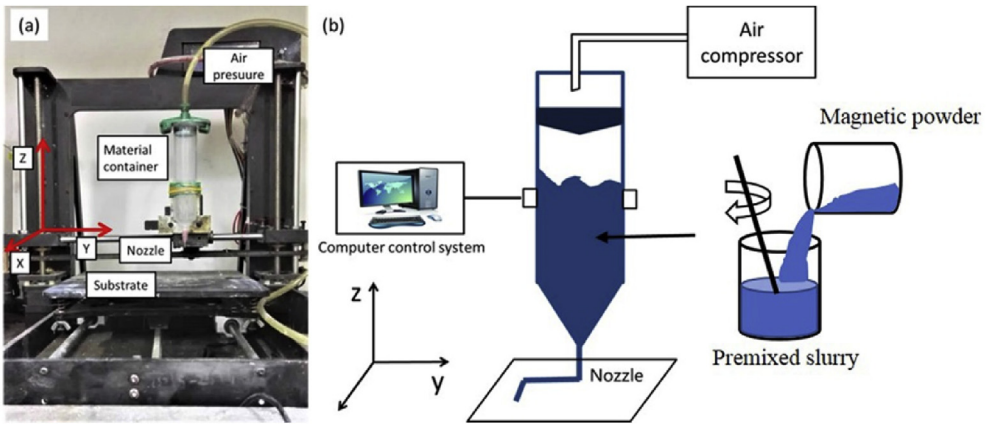

Fig. 2. The (a) 3D printing equipment and (b) 3D printing schematic diagram for printing NdFeB-based bonded magnets.

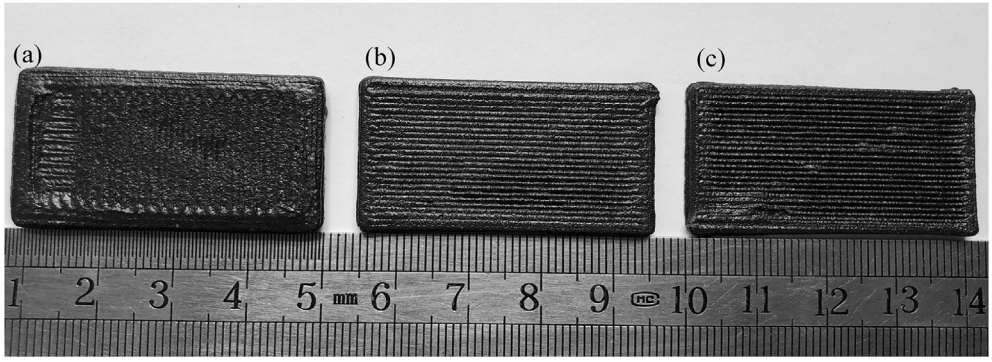

Fig. 3. 3D printed NdFeB bonded magnets with: (a) 0 wt.%, (b) 20 wt.%, (c) 25 wt.% $SrFe_{12}O_{19}$ addition.

coarse particle size (75 μm) of NdFeB powder, the distribution of NdFeB powder in the ferrite-free slurry was non-uniform, and the printing appearance of the ferrite-free printed magnets was not good. Printed lines overlapped and even collapsed. There was difficulty in maintaining the designed shape during printing with bulges, pits, and pores, as shown in Fig. 3(a). Slurries with pseudoplastic behavior are highly desirable in controlling the forming shape, which can flow at high shear rates induced by pressure and after forming it is fixed in a defined position. That means, the slurries retain their shape without deformation [27,28]. It has been reported that the rheological behavior of the slurry can be controlled with fine ferrite powder addition [29]. Therefore, different amounts of $SrFe_{12}O_{19}$ were mixed with NdFeB to prepare highly loaded printing slurries. With the $SrFe_{12}O_{19}$ addition, the slurries exhibited better pseudoplastic behavior, as shown in Fig. 4. With 20 wt.% $SrFe_{12}O_{19}$ addition, the printed magnets had good dimensional accuracy and surface quality, as shown in Fig. 3(b). Upon further increasing the $SrFe_{12}O_{19}$ content to 25 wt.%, the viscosity was too high for the slurry to flow out from the nozzle, resulting in low dimensional accuracy and poor surface quality. From Fig. 3(c), discontinuous printing trajectory was observed in the printed magnets. In addition, the width between printed lines was much larger than the nozzle diameter with obvious gaps between the printed lines.

The printing speed, layer height, and nozzle diameter are the key factors for the printing quality. The optimized printing parameters for printing NdFeB bonded magnets with a high printing accuracy are listed in Table 2. A rectangular block as an example was printed, shown in Fig. 5(a). The printed lines are observed while there is no defect or deformation on the surface in Fig. 5(b) and (c), which illustrates that the hybrid slurry is suitable for printing. After being extruded and deposited on the print platform, the shape of the slurry filament changed from cylindrical to elliptic cylindrical because of its own weight and rheological behavior. The printed lines can be obviously observed. The top surface was homogenous, and the width between adjacent two printed lines was close to 0.6 mm nozzle diameter, while the layer height was close to 0.45 mm.

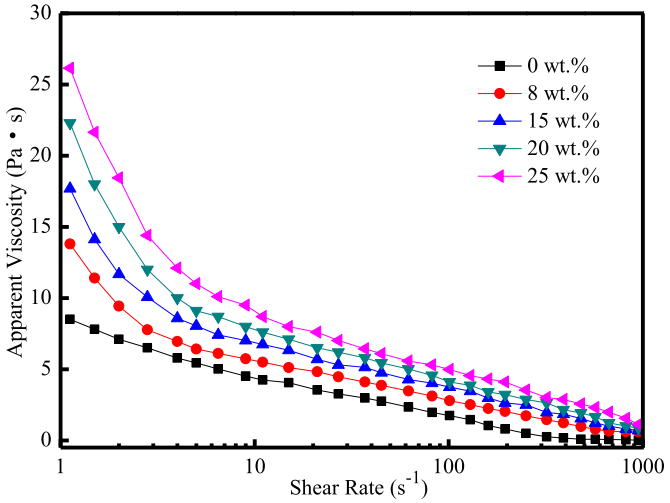

Fig. 4. Viscosity of printing slurry with different amounts of $SrFe_{12}O_{19}$ as a function of shear rate.

Table 2
3D printing parameters for printing NdFeB bonded magnets.

Printing parameter	Value
Layer height	0.45 mm
Nozzle diameter	0.6 mm
Printer speed	30 mm/s
Fill density	95%
Fill pattern	Rectilinear
Bed temp.	25 °C

The printing height map of the printed magnets was observed by a confocal laser scanning microscope. The same green color presented in Fig. 6(a) corresponded to the printed peaks, while the blue color corresponded to the printed valleys, indicating that there were at a similar height. Overall, the surface quality of the printed magnets was good, which was consistent with the results shown in Fig. 3(b). The surface roughness was ~6 μm, as shown in Fig. 6(b), and the surface profile curve also shows the printed lines. Besides, the surface roughness of parts produced by different AM processes is also listed in Table 3. The roughness of printed NdFeB bonded magnets was much lower compared with other AM methods.

3.2. Microstructure

The printed magnets had a homogeneous microstructure and relatively high density due to the highly loaded slurry. The micrograph in Fig. 7(a) indicates uniform dispersion of the magnetic particles in the printed magnets. Typical microstructure of the bonded magnets is shown in Fig. 7(b), in which the dark regions

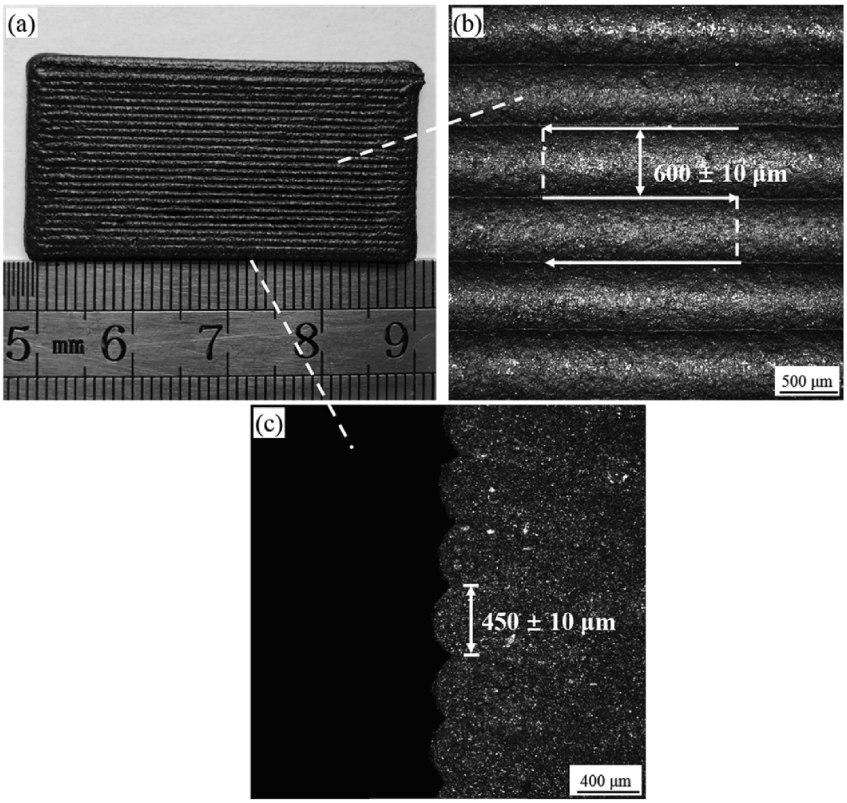

Fig. 5. The printed NdFeB bonded magnets with 20 wt.% $SrFe_{12}O_{19}$ addition: (a) overview, (b) CLSM morphology of the top surface, and (c) CLSM morphology of the side surface.

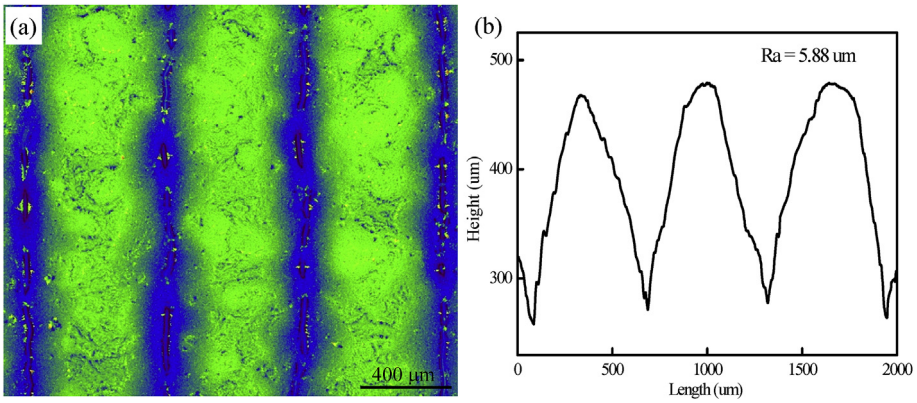

Fig. 6. (a) Height map, and (b) the surface roughness curve of the printed NdFeB bonded magnets with 20 wt.% $SrFe_{12}O_{19}$ addition.

Table 3
The top surface roughness of parts produced by different AM printing process.

Process	Material	Ra/μm
Material jetting	NdFeB bonded magnets	5.88
FDM [30]	ABS	24.7
SLS [31]	Polyamide	10.47
SLM [32]	316L	13.12
EBSM [33]	316L	7.9

correspond to the epoxy resin binder. Two types of grey regions can also be recognized. The EDS results demonstrate that the region 'A' corresponds to the NdFeB particle, while the region 'B' is corresponding to the $SrFe_{12}O_{19}$ particle. The plate-shaped ~75 μm NdFeB particles were separated by the epoxy resin and fine ~1 μm $SrFe_{12}O_{19}$ particles.

Fig. 8 shows the fracture morphology of the printed magnets taken from different regions. No discrete interfaces between filaments can be identified, and there were no obvious defects or pores observed from the fracture morphology, which indicated good coalescence of the printed filaments. During printing, the deposited slurry spread out to fill the space between the printed lines before curing. Then, the epoxy resin formed physical cross-links between layers, which can result in significantly better transverse strength. The ultimate tensile strength (UTS) was 12 ± 0.7 MPa for the printed NdFeB bonded magnets with 20 wt.% $SrFe_{12}O_{19}$. It has been reported that the UTS for AM printed magnets was commonly about 7 MPa [16]. Generally, the tensile strength of the NdFeB bonded magnets strongly depends on the magnetic powder loading fraction and the powder shape [2]. Besides, the UTS also depends on the matrix material, filler shape, filler content, additives, temperature and slicing algorithm, etc. The magnets made of irregular melt-spun powders exhibited higher tensile strength compared to atomized spherical powders [34]. Therefore, the relatively high UTS of the printed hybrid bonded magnets may be attributed to the highly loaded printing slurry, binder epoxy

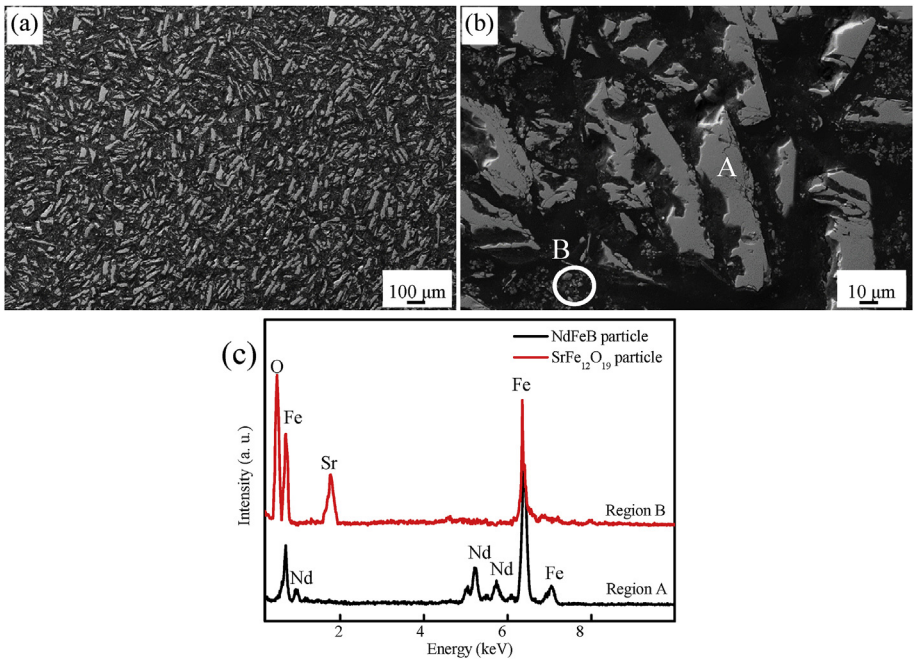

Fig. 7. SEM images of the printed NdFeB bonded magnets with 20 wt.% $SrFe_{12}O_{19}$ addition: (a) overview, (b) detail, and (c) the correspond EDS patterns of region 'A' and 'B'.

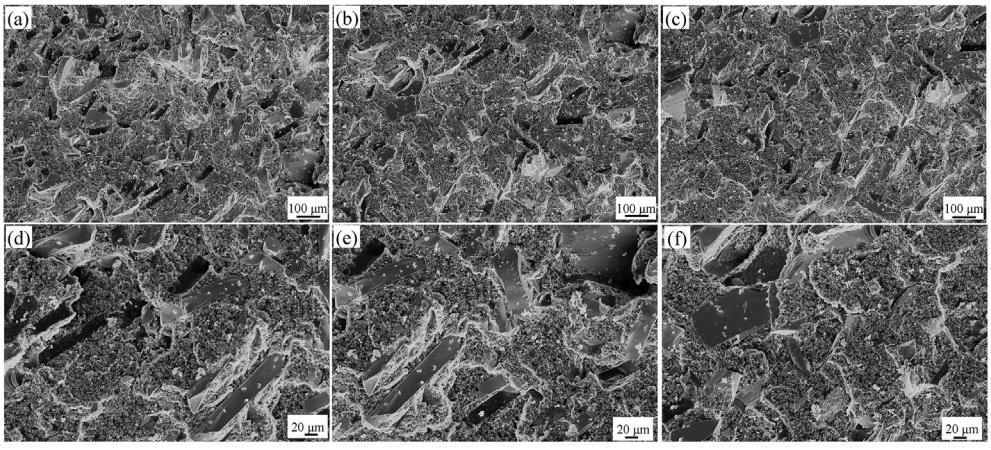

Fig. 8. The fracture morphology of the printed NdFeB bonded magnets with 20 wt.% $SrFe_{12}O_{19}$ taken from different regions at (a), (b), (c) low and (d), (e), (f) high magnification.

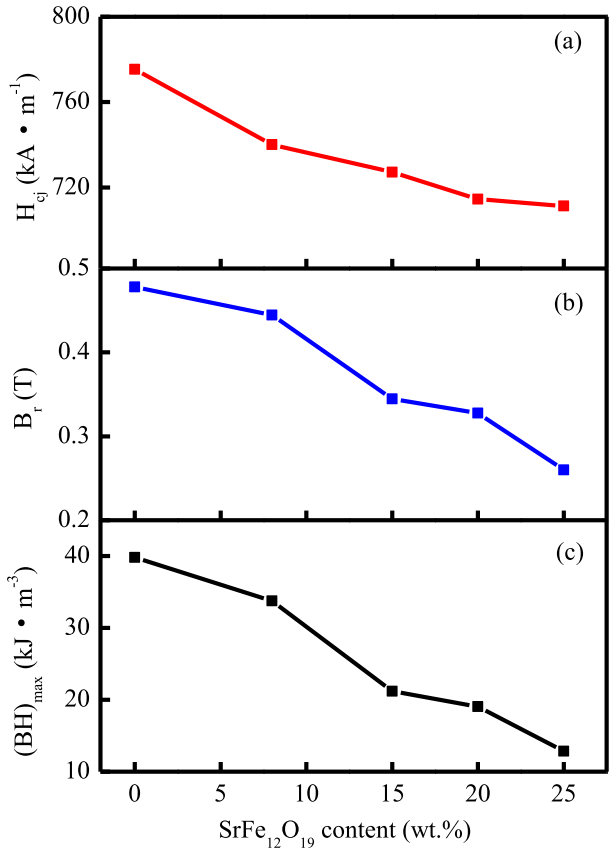

Fig. 9. Variations of the (a) coercivity, (b) remanence, and (c) maximum magnetic energy product for the printed NdFeB bonded magnets as a function of $SrFe_{12}O_{19}$ content.

resin and the introduction of fine ferrite powder and irregular NdFeB powder.

3.3. Magnetic properties

Fig. 9 presents the magnetic properties of the as-printed NdFeB bonded magnets as a function of the $SrFe_{12}O_{19}$ content. In the printed ferrite-free bonded magnets, the measured coercivity H_{cj}, remanence B_r and maximum magnetic energy product $(BH)_{max}$ values were 775.3 kA/m, 0.478 T, and 39.78 kJ/m^3, respectively. The characteristics of the $SrFe_{12}O_{19}$ powder are: $H_{cj} = 263–295$ kA/m, $Br = 0.405–0.415$ T, $(BH)_{max} = 30.3–31.9$ kJ/m^3, which are much lower than the NdFeB powder ($H_{cj} = 779$ kA/m, $Br = 0.862$ T, $(BH)_{max} = 113.3$ kJ/m^3). With 8 wt.% $SrFe_{12}O_{19}$ addition, the

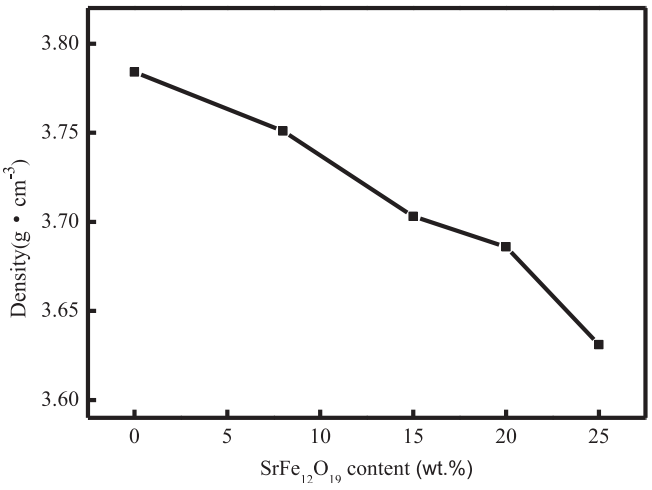

Fig. 10. Density of printed NdFeB bonded magnets with different $SrFe_{12}O_{19}$ addition.

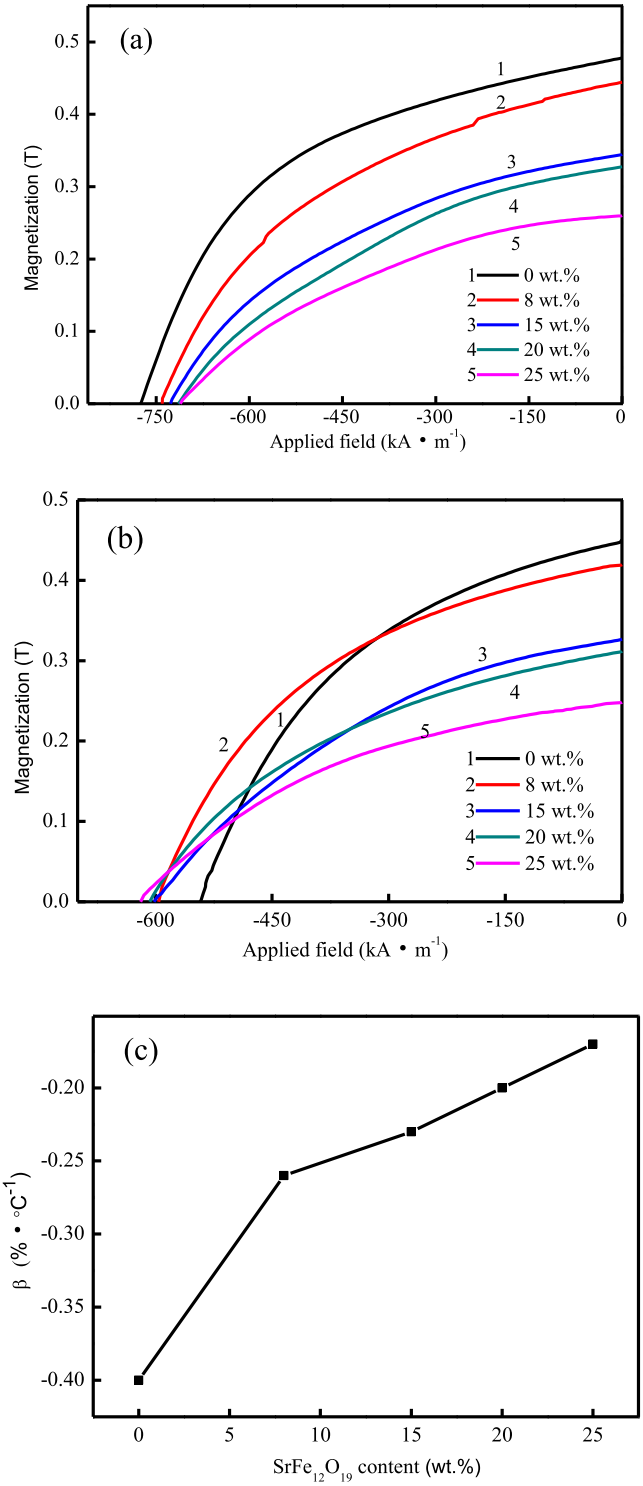

Fig. 11. Demagnetization curves for the printed NdFeB bonded magnets with different amounts of $SrFe_{12}O_{19}$ at (a) 25 °C and (b) 100 °C, and (c) the coercivity temperature coefficients (from 25 to 100 °C) of the printed magnets.

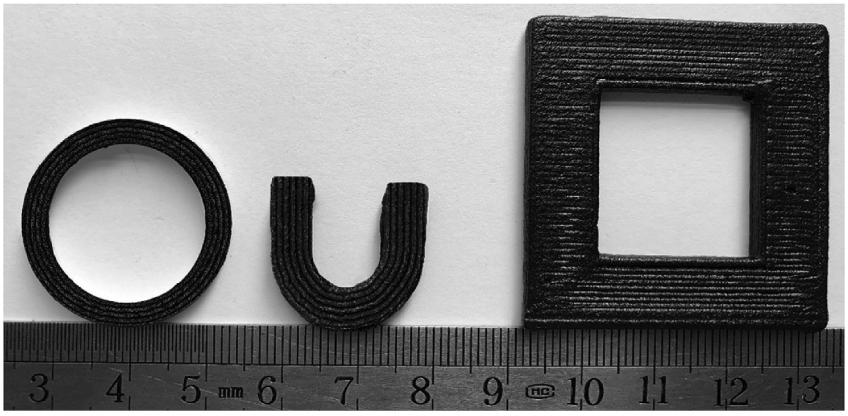

Fig. 12. Complex-shaped NdFeB bonded magnets with 20 wt.% $SrFe_{12}O_{19}$ prepared by 3D printing.

corresponding H_{cj}, B_r and $(BH)_{max}$ were 740.1 kA/m, 0.444 T and 33.73 kJ/m^3, respectively. It can be clearly seen that the magnetic properties of the printed hybrid bonded magnets decreased as the $SrFe_{12}O_{19}$ content increased. The variation tendency in magnetic properties is consistent with that reported in Ref. [35] for the NdFeB/ferrite hybrid magnets. These changes are caused by a lower content of NdFeB powder in the magnetic volume and lower values of magnetic parameters for the $SrFe_{12}O_{19}$ powder. Note that there is basically no degradation in the intrinsic coercivity in the printed ferrite-free NdFeB bonded magnets. This result is consistent with that reported in Ref. 24.

The density of the printed magnets is essential to ensure magnetic functionality, as it determines the magnetic flux the magnets can generate in a given space. The measured density of the printed NdFeB bonded magnets is shown in Fig. 10 as a function of the $SrFe_{12}O_{19}$ content. Here, the measured density of the ferrite-free magnets was 3.78 g/cm^3. This is nearly 98% dense compared to the theoretical density of 3.84 g/cm^3, which can be calculated from the starting nominal composition of 83.1 wt.% loading fraction of magnetic particles in the epoxy resin. The $SrFe_{12}O_{19}$ density is 5.5 g/cm^3. With the increase of the $SrFe_{12}O_{19}$ content, the density of the printed hybrid magnets decreased, as seen in Fig. 10. However, the relative density of all printed ferrite-containing magnets still reached 98% compared to the theoretical density, indicating a lower level of porosity in 3D printed magnets. Huber et al. reported that the density of 3D printed NdFeB bonded magnets was 3.57 g/cm^3 [21]. Ref. 21 reported the printed NdFeB bonded magnets with the PA11 as a binder. Due to the difference in raw material compositions, there was a difference in the printed density. Besides, in this study, fine $SrFe_{12}O_{19}$ particles filled in the voids between the larger NdFeB particles and hence improved the density of the printed magnets. Therefore, the relatively high density of the printed NdFeB/$SrFe_{12}O_{19}$ bonded magnets was attributed to the highly loaded printing slurry.

In real applications, the magnets are frequently exposed to elevated temperatures. Therefore, the magnetic properties of the hybrid bonded magnets were investigated in the 25–100 °C temperature range. Fig. 11(a) and (b) show the demagnetization curves for the printed NdFeB bonded magnets with different amounts of $SrFe_{12}O_{19}$ at 25 °C and at 100 °C, respectively. With the increase of the $SrFe_{12}O_{19}$ content, the room temperature magnetic properties decreased, which is consistent with the results shown in Fig. 9. In addition, all the magnetic parameters of the printed magnets decreased with increasing temperature due to their poor thermal stability. However, the decreasing rate of the intrinsic coercivity of the ferrite-containing magnets was much lower than the ferrite-free magnets. This may indicate that the thermal stability of the magnets was effectively improved through the $SrFe_{12}O_{19}$ introduction. Furthermore, the coercivity temperature coefficients of the printed hybrid bonded magnets in the 25–100 °C temperature range, which were calculated based on the data in Fig. 11(a) and (b), are shown in Fig. 11(c). It can be seen that the corresponding β values were improved from −0.4%/°C to −0.17%/°C in the 25–100 °C range by adding 25 wt.% $SrFe_{12}O_{19}$. Since the coercivity temperature coefficient for the strontium ferrite magnets is positive, the improvement of β can be achieved in the hybrid magnets.

The above results indicate that such type of hybrid magnets has better thermal stability, giving rise to their extended application at elevated temperatures. For this reason, the hybrid NdFeB/$SrFe_{12}O_{19}$ bonded magnets are promising candidates for applications in motors, generator, and sensor, in which the obtainable magnetic properties are sufficient and the operating temperature is relatively high.

3.4. 3D printed parts

Fig. 12 shows several complex-shaped NdFeB bonded magnets with 20 wt.% ferrite prepared by the 3D printing process. Square, ring, horseshoe-type 3D magnet structures were printed with good dimensional accuracy and surface quality. This implied that the 3D printing process can be employed to prepare near-net shaped magnets. Compared to available 3D printed magnets, the hybrid NdFeB/$SrFe_{12}O_{19}$ printed magnets have a high relative density of nearly 98%, low surface roughness ~6 μm, and better thermal stability. With the fine $SrFe_{12}O_{19}$ addition, the voids between the larger NdFeB particles were filled, resulting in the improvement of the relative density of the printed magnets. Besides, the coercivity temperature coefficient of the $SrFe_{12}O_{19}$ magnets was positive. Consequently, the thermal stability was significantly improved in the hybrid magnets. Since NdFeB bonded magnets have broad applications, the combination of 3D printing and hybrid NdFeB/$SrFe_{12}O_{19}$ bonded magnets unlocks the full design potential of the magnets and further broadens the scope of their application. The freedom in magnet body shape and size for 3D printed magnets gives rise to advantages in terms of reducing RE material waste and reducing post-manufacturing costs.

4. Conclusions

In this study, complex-shaped NdFeB bonded magnets with $SrFe_{12}O_{19}$ addition have been prepared by 3D printing. Highly loaded pseudo-plastic printing slurries were employed to print

bonded magnets with a high relative density of >98%. With 20 wt.% $SrFe_{12}O_{19}$ addition, the printed magnets obtained good dimensional accuracy and surface quality. The corresponding surface roughness was ~6 μm. Good coalescence of the printed filaments was observed. The addition of $SrFe_{12}O_{19}$ to NdFeB bonded magnets caused a decrease in magnetic properties in comparison with the pure NdFeB bonded magnets. Conversely, the coercivity temperature coefficient β increased from −0.4%/°C to −0.17%/°C by increasing $SrFe_{12}O_{19}$ content from 0 wt.% to 25 wt.%, indicating the enhancement of thermal stability of the hybrid bonded magnets. Therefore, the 3D printed NdFeB based bonded magnets may have broad applications at elevated operating temperatures, with minimum tooling cost and RE materials waste.

Acknowledgments

This work was supported by the Fundamental Research Funds for the Central Universities, China (No. FRF-TP-18-025A1) and the State Key Lab for Advanced Metals and Materials, China (No. 2016-ZD02).

References

[1] O. Gutfleisch, M.A. Willard, E. Bruck, C.H. Chen, S.G. Sankar, J.P. Liu, Magnetic materials and devices for the 21st century: stronger, lighter, and more energy efficient, Adv. Mater. 23 (2011) 821–842.
[2] L. Li, A. Tirado, I.C. Nlebedim, O. Rios, B. Post, V. Kunc, R.R. Lowden, E. Lara-Curzio, R. Fredette, J. Ormerod, T.A. Lograsso, M.P. Paranthaman, Big area additive manufacturing of high performance bonded NdFeB magnets, Sci. Rep. 6 (2016) 36212.
[3] A.K. Pathak, K.A. Gschneidner Jr., M. Khan, R.W. McCallum, V.K. Pecharsky, High performance Nd-Fe-B permanent magnets without critical elements, J. Alloys Compd. 668 (2016) 80–86.
[4] J.M.D. Coey, Permanent magnets: plugging the gap, Scr. Mater. 67 (2012) 524–529.
[5] T. Xu, H. Peng, Formation cause, composition analysis and comprehensive utilization of rare earth solid wastes, J. Rare Earth. 27 (2009) 1096–1102.
[6] J. Ormerod, S. Constantinides, Bonded permanent magnets: current status and furure opportunities (invited), J. Appl. Phys. 81 (1997) 4816.
[7] I.C. Nlebedim, H. Ucar, C.B. Hatter, R.W. McCallum, S.K. MaCall, M.J. Kramer, M.P. Paranthamn, Studies on in situ magnetic alignment of bonded anisotropic Nd-Fe-B alloy powders, J. Magn. Magn Mater. 422 (2017) 168–173.
[8] B.M. Ma, J.W. Herchenroeder, B. Smith, M. Suda, D.N. Brown, Z. Chen, Recent development in bonded NdFeB magnets, J. Magn. Magn Mater. 239 (2002) 418–423.
[9] D. Plusa, B. Slusarek, M. Dospial, U. Kotlarczyk, T. Mydlarz, Magnetic properties of anisotropic Nd-Fe-B resin bonded magnets, J. Alloys Compd. 423 (2006) 81–83.
[10] F.Q. Zhai, A.Z. Sun, D. Yuan, J. Wang, S. Wu, A.A. Volinsky, Z.X. Wang, Epoxy resin effect on anisotropic Nd-Fe-B rubber-bonded magnets performance, J. Alloys Compd. 509 (2011) 687–690.
[11] M.P. Paranthamn, C.S. Shafer, A.M. Elliott, D.H. Siddel, M.A. McGuire, R.M. Springfield, J. Martin, R. Fredette, J. Ormerod, Binder jetting: a novel NdFeB bonded magnet fabrication process, JOM 68 (2016) 1978–1982.
[12] S. Kumar, J.P. Kruth, Composites by rapid prototyping technology, Mater. Des. 31 (2010) 850–856.
[13] L. Santana, J.L. Alves, A. da C.S. Netto, A study of parametric calibration for low cost 3D printing: seeking improvement in dimensional quality, Mater. Des. 135 (2017) 159–172.
[14] M. Bodaghi, A.R. Damanpack, G.F. Hu, W.H. Liao, Large deformations of soft metamaterials fabricated by 3D printing, Mater. Des. 131 (2017) 81–91.
[15] T.D. Ngo, A. Kashani, G. Imbalzano, K.T.Q. Nguyen, D. Hui, Additive manufacturing (3D printing): a review of materials, methods, applications and challenges, Compos. Part. B. Eng. 143 (2018) 172–196.
[16] L. Li, B. Post, V. Kunc, A.M. Elliott, M.P. Paranthaman, Additive manufacturing of near-net-shape bonded magnets: prospects and challenges, Scr. Mater. 135 (2017) 100–104.
[17] B.G. Compton, J.A. Lewis, 3D-printing of lightweight cellular composites, Adv. Mater. 26 (2014) 5930–5935.
[18] K. Sun, T.S. Wei, B.Y. Ahn, J.Y. Seo, S.J. Dillon, J.A. Lewis, 3D printing of interdigitated li0ion microbattery architectures, Adv. Mater. 25 (2013) 4539–4543.
[19] A.E. Jakus, S.L. Taylor, N.R. Geisendorfer, D.C. Dunand, R.N. Shah, Metallic architectures from 3D-printed powder-based liquid inks, Adv. Funct. Mater. 25 (2015) 6985–6995.
[20] S.L. Morissette, J.A. Lewis, J. Cesarano, D.B. Dimos, T.Y. Baer, Solid freeform fabrication of aqueous alumina-poly(vinyl alcohol) gelcasting suspensions, J. Am. Ceram. Soc. 83 (2000) 2409–2416.
[21] C. Huber, C. Abert, F. Bruckner, M. Groenefeld, O. Muthsam, S. Schuschnigg, K. Sirak, R. Thanhoffer, I. Teliban, C. Vogler, R. Windl, D. Suess, 3D print of polymer bonded rare-earth magnets, and 3D magnetic field scanning with an end-user 3D printer, Appl. Phys. Lett. 109 (2016) 162401.
[22] J.L. Wang, H.M. Xie, L. Wang, T. Senthil, R. Wang, Y.D. Zheng, L.X. Wu, Anti-gravitational 3D printing of polycaprolactone-bonded Nd-Fe-B based on fused deposition modeling, J. Alloys Compd. 715 (2017) 146–153.
[23] B.G. Compton, J.W. Kemp, T.V. Novikov, R.C. Pack, C.I. Nlebedim, C.E. Duty, O. Rios, M.P. Paranthaman, Direct-write 3D printing of NdFeB bonded magnets, Mater. Manuf. Process. 33 (2018) 109–113.
[24] L. Li, A. Tirado, B.S. Conner, M.F. Chi, A.M. Elliott, O. Rios, H.D. Zhou, M.P. Paranthaman, A novel method combining additive manufacturing and alloy infiltration for NdFeB bonded magnet fabrication, J. Magn. Magn Mater. 438 (2017) 163–167.
[25] M. Dospial, D. Plusa, Magnetization reversal processes in bonded magnets made from a mixture of Nd-(Fe,Co)-B and strontium ferrite powders, J. Magn. Magn Mater. 330 (2013) 152–158.
[26] K. Gandha, L. Li, I.C. Nlebedim, B.K. Post, V. Kunc, B.C. Sales, J. Bell, M.P. Paranthaman, Additive manufacturing of anisotropic hybrid NdFeB-SmFeN nylon composite bonded magnets, J. Magn. Magn Mater. 467 (2018) 8–13.
[27] J.W. Wang, L.L. Shaw, Rheological and extrusion behavior of dental porcelain slurries for rapid prototyping applications, Mater. Sci. Eng. 397 (2005) 314–321.
[28] U. Scheithauer, E. Schwarzer, H. Richter, T. Moritz, Thermoplastic 3D printing-An additive manufacturing method for producing dense ceramics, Int. J. Appl. Ceram. Technol. 12 (2015) 26–31.
[29] S. Mousavian, H. Ebadi-Dehaghani, D. Ashouri, H. Sadeghipour, F. Jabbari, Effect of polymer matrix on the magnetic properties of polymer bonded magnets filled Fe_3O_4 nanoparticles, J. Polym. Res. 19 (2012) 1–9.
[30] C.J.L. Perez, Analysis of the surface roughness and dimensional accuracy capability of fused deposition modeling process, Int. J. Prod. Res. 40 (2001) 2865–2881.
[31] A. Sachdeva, S. Singh, V.S. Sharma, Investigating surface roughness of parts produced by SLS process, Int. J. Adv. Manuf. Technol. 64 (2013) 1505–1516.
[32] G. Strano, L. Hao, R.M. Everson, K.E. Evans, Surface roughness analysis, modelling and prediction in selective laser melting, J. Mater. Process. Technol. 213 (2013) 589–597.
[33] C. Guo, F. Lin, W. Ge, Study on the fabrication process of 316L stainless steel via electron beam selective melting, Chin. J. Mech. Eng. 50 (2014) 152–153.
[34] M.G. Garrell, A.J. Shih, B.M. Ma, E. Lara-Curzio, R.O. Scattergood, Mechanical properties of nylon-bonded Nd-Fe-B permanent magnets, J. Magn. Magn Mater. 257 (2003) 32–43.
[35] X.F. Wang, D. Lee, Z.L. Jiang, Magnetic properties of hybrid polymer bonded Nd-Fe-B/ferrite magnets, J. Appl. Phys. 99 (2006), 08B513.